

Leakage Current of a Superconductor-Normal Metal Tunnel Junction Connected to a High-Temperature Environment

A. Di Marco,¹ V. F. Maisi,^{2,3} J. P. Pekola,³ and F. W. J. Hekking¹

¹*LPMMC-CNRS, Université Joseph Fourier, 25 Avenue des Martyrs BP166 38042 Grenoble Cedex, France*

²*Centre for Metrology and Accreditation (MIKES), P.O. Box 9, 02151 Espoo, Finland*

³*Low Temperature Laboratory, Aalto University, P.O. Box 13500, FI-00076 Aalto, Finland*

(Dated: November 18, 2021)

We consider a voltage-biased Normal metal-Insulator-Superconductor (NIS) tunnel junction, connected to a high-temperature external electromagnetic environment. This model system features the commonly observed subgap leakage current in NIS junctions through photon-assisted tunneling which is detrimental for applications. We first consider a NIS junction directly coupled to the environment and analyze the subgap leakage current both analytically and numerically; we discuss the link with the phenomenological Dynes parameter. Then we focus on a circuit where a low-temperature lossy transmission line is inserted between the NIS junction and the environment. We show that the subgap leakage current is exponentially suppressed as the length, ℓ , and the resistance per unit length, R_0 , of the line are increased. We finally discuss our results in view of the performance of NIS junctions in applications.

PACS numbers: 74.55.+v, 74.25.F-, 85.25.Am, 72.70.+m

I. INTRODUCTION

The peculiar nature of single-particle electronic transport through a normal metal-insulator-superconductor (NIS) junction is at the origin of several interesting applications. Such junctions are widely used in experiments of mesoscopic physics as a spectroscopic tool^{1,2}, as a very sensitive thermometer³⁻⁵ and as a key element in nano-refrigeration^{3,6,7}. Furthermore, NIS junctions are currently investigated in view of achieving a high accuracy when controlling the current through a single-electron SINIS turnstile. Such a device is one of the interesting candidates for the completion of the so-called quantum metrological triangle, *i.e.*, it can be used to obtain a precise realization of current^{8,9}. These applications are all based on the existence of the Bardeen-Cooper-Schrieffer (BCS) energy gap Δ in the density of states (DoS) of the superconductor¹⁰. Ideally one would expect no single-electron current to flow through a NIS junction at low temperature as long as the bias voltage V satisfies the inequality $-\Delta < eV < \Delta$.

In practice the subgap current is different from zero. This is a central problem which limits the performance of applications based on energy-selective single-particle transport in NIS junctions. The presence of unwanted accessible states in the subgap region manifests itself as a smearing of the junction's current-voltage (I - V) characteristic as well as of its differential conductance. Giaever was the first to experimentally study the NIS junction. He noticed that this deviation from the ideal behavior was present even if the junction was kept at a temperature much lower than the critical one T_c of the superconductor¹¹. A possible source of subgap leakage currents is the occurrence of many-electron tunneling processes, such as Andreev reflection¹²⁻¹⁴. However, these many-electron processes are strongly suppressed if the tunnel resistance R_T of the junction is chosen high

enough and do not account for the observed residual subgap transport either.

Dynes modified the BCS superconducting DoS introducing a phenomenological dimensionless parameter, γ_{Dynes} , in order to fit the behavior of the subgap quasi-particle tunneling current through a Josephson junction¹⁵. The modified DoS, normalized to the corresponding normal-state DoS at the Fermi energy, is given by

$$N_S^{\text{Dynes}} = \left| \Re \left[\frac{E/\Delta + i\gamma_{\text{Dynes}}}{\sqrt{(E/\Delta + i\gamma_{\text{Dynes}})^2 - 1}} \right] \right|. \quad (1)$$

It can be seen that γ_{Dynes} indeed accounts for the broadening of the DoS around Δ and the occurrence of states within the gap. This expression is frequently used in both numerical and analytical calculations, but concerning the microscopic origin of the Dynes parameter γ_{Dynes} , for temperatures far below T_c , relatively little is known.

Recently it was realized that the exchange of energy between the NIS junction and its surrounding electromagnetic environment may give rise to subgap features similar to those accounted for phenomenologically by the Dynes parameter^{16,17}. Indeed, under certain conditions, energy absorption from such an environment enables the crossing of the tunnel barrier by single electrons even for $|V|$ much less than Δ/e . Within this framework an analytical expression for γ_{Dynes} has been obtained in terms of parameters characterizing the NIS junction's environment for the special case of a purely resistive external circuit¹⁶.

Following the idea of photon-assisted tunneling demonstrated in Ref. 16, we generalize the approach here and obtain expressions for the subgap leakage current and the Dynes parameter valid for an external circuit characterized by an arbitrary impedance $Z(\omega)$, kept at a temperature T_{env} that is not necessarily the temperature T_{jun}

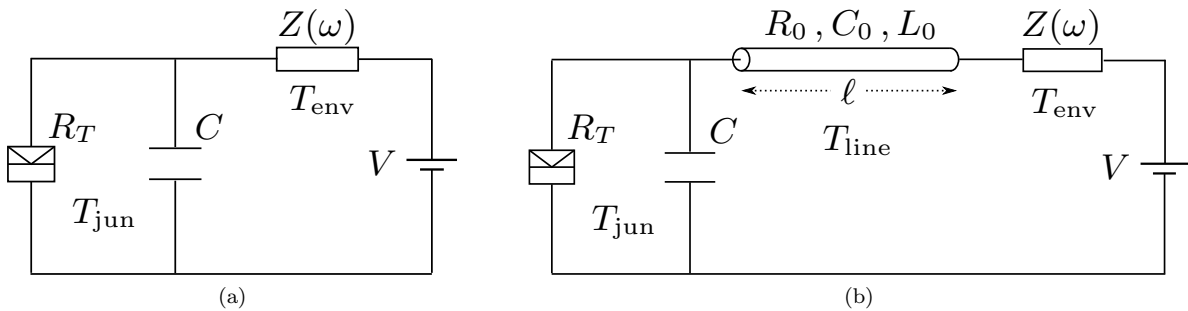


FIG. 1: Circuit representation of the two configurations studied in this paper. (a) A NIS junction at temperature T_{jun} is connected in parallel to its capacitance C and to an impedance $Z(\omega)$ which represents the high-temperature environment at temperature $T_{\text{env}} \gg T_{\text{jun}}$. The whole circuit is biased by the constant voltage V . (b) A transmission line of length ℓ is inserted between the junction and the impedance $Z(\omega)$ of circuit (a). It is described by the parameters R_0 , C_0 and L_0 , the resistance, the capacitance and the inductance per unit length, respectively, as well as by its temperature which is assumed equal to T_{jun} .

of the NIS junction, see Fig. 1(a). Then we turn our attention to the circuit depicted in Fig. 1(b), where we study the effects of the insertion of a lossy transmission line, meant to act as a filter, between the cold junction and the high-temperature external impedance $Z(\omega)$. In particular we use our results to understand under which conditions the transmission line will behave as a filter capable of reducing the photon-assisted tunneling induced by the high-temperature external impedance and thus reducing the Dynes parameter to values that are compatible with the accuracy requirements for applications such as the SINIS turnstile.

II. NIS JUNCTION COUPLED TO A HIGH-TEMPERATURE ENVIRONMENT

A. Single-Particle Current

We start by considering the basic circuit illustrated in Fig. 1(a) where a NIS junction is connected in series to an effective high-temperature impedance $Z(\omega)$. The junction itself is characterized by a tunnel resistance R_T in parallel with a capacitance C . The entire circuit is voltage biased. This constitutes a minimal model for a junction embedded in an external electromagnetic environment at temperature T_{env} , which can be much higher than the temperature T_{jun} of the junction.

According to the so-called $P(E)$ theory¹⁸, the single-particle tunneling current through a NIS junction coupled to an external environment is given by

$$I_{\text{NS}}(V) = \frac{1}{eR_T} \int dE \int dE' N_S(E') [1 - f(E')] \times \left\{ f(E - eV) - f(E + eV) \right\} P(E - E'). \quad (2)$$

Here, the energy E refers to the electrons of the normal metal, E' is the energy of the superconductor quasiparticles, $N_S(E')$ is the BCS density of states of the

superconducting wire divided by the normal-metal DoS at the Fermi level and $f(E) = [e^{\beta_{\text{jun}} E} + 1]^{-1}$ is the Fermi-Dirac distribution with $\beta_{\text{jun}} = 1/k_B T_{\text{jun}}$ the inverse temperature of the junction. Expression (2) does not take into account the higher order processes in tunneling which will be ignored throughout this paper. The validity of this assumption will be discussed in Sec.IV.

The function $P(E)$ in Eq. (2) is the probability density that the tunneling electron exchanges an amount of energy E with the environment. This process takes place through the emission or absorption of photons. It is defined as

$$P(E) = \frac{1}{2\pi\hbar} \int_{-\infty}^{+\infty} dt e^{iEt/\hbar} e^{J(t)}, \quad (3)$$

i.e., it is the Fourier transform of the exponential of the correlation function

$$J(t) = 2 \int_0^{+\infty} \frac{d\omega}{\omega} \frac{\Re[Z_{\text{tot}}(\omega)]}{R_K} \times \left\{ \coth\left(\frac{1}{2}\beta_{\text{env}}\hbar\omega\right) [\cos(\omega t) - 1] - i \sin(\omega t) \right\}. \quad (4)$$

Here $Z_{\text{tot}}(\omega)$ is the total impedance seen by the junction, resulting from the connection in parallel of C and $Z(\omega)$, $R_K = h/e^2$ is the quantum resistance and $\beta_{\text{env}} = 1/k_B T_{\text{env}}$.

The function $J(t)$ determines the strength of the coupling between the NIS junction and the environment. Indeed if $J(t) = 0$, the probability density $P(E)$ is equal to a Dirac delta $\delta(E)$ and the single-particle tunneling current is elastic. Expression (2) then reduces to the standard expression for single-particle tunneling in NIS junctions valid in the absence of environment. The environment-induced inelastic tunneling processes occur only when $J(t) \neq 0$. In general, the time intervals where the inelastic effects are important are related to the energy ranges where $P(E) \neq 0$. Depending on the value of

$J(t)$, the coupling between the NIS junction and the environment can be considered weak or strong. Throughout this paper we will treat both regimes of weak and strong coupling in more detail.

In order to analyze the smearing of the NIS junction's I - V characteristic due to the presence of the high-temperature environment, we will ignore the thermal smearing induced by finite temperature of the N and S electrodes. This is an adequate approximation under standard experimental conditions where $T_{\text{jun}} \ll \Delta/k_B$. Hereafter we will set the temperature of the junction T_{jun} to zero. Under this assumption the single-particle current (2) becomes

$$I_{\text{NS}}(V) \simeq \frac{1}{eR_T} \int_{-eV}^{+eV} dE \int_{\Delta}^{+\infty} dE' N_S(E') P(E - E'). \quad (5)$$

We furthermore will focus on the subgap region of the I - V curve considering $|eV| \ll \Delta$. As a result, the integration variables $|E| \ll E'$ in (5), and we can approximate $P(E - E') \approx P(-E')$. The resulting integral over E can be performed immediately to yield

$$I_{\text{NS}}^{\text{sub}}(V) \simeq \Gamma \frac{V}{R_T}, \quad (6)$$

where the factor Γ is given by the integral

$$\Gamma = 2 \int_{\Delta}^{+\infty} dE' N_S(E') P(-E'). \quad (7)$$

We see that for the parameter Γ , Eq. (7), and hence the subgap current given by Eq. (6) to be nonzero, the function $P(E)$ should be nonzero for energies $E \leq -\Delta$. This reflects the fact that under subgap conditions $eV, k_B T_{\text{jun}} \ll \Delta$, a nonzero single-particle current occurs only if the tunneling electrons absorb an energy $\gtrsim \Delta$ from the environment. For instance, $\Gamma = 0$ for elastic tunneling in the absence of an environment, when $P(E) = \delta(E)$. We also expect Γ to vanish when the temperature of the environment $k_B T_{\text{env}}$ is much less than the energy gap Δ . Indeed, due to detailed balance¹⁸, $P(-E) = e^{-E/k_B T_{\text{env}}} P(E)$, the function $P(E)$ is strongly suppressed for negative energies $E < -k_B T_{\text{env}}$. This means that the integral in (7) will vanish unless the environment is sufficiently hot, $k_B T_{\text{env}} \gtrsim \Delta$.

In order to make a connection with the aforementioned approach due to Dynes, we linearize the usual expression for elastic single-particle tunneling in a NIS junction, using the Dynes DoS (1) to characterize the superconducting electrode. One obtains the linear subgap current-voltage relationship

$$I_{\text{NS}}^{\text{sub}}(V) \simeq \sqrt{\frac{\gamma_{\text{Dynes}}^2}{\gamma_{\text{Dynes}}^2 + 1}} \frac{V}{R_T}.$$

Comparing this result with Eq. (6) above, we conclude that, in the linear regime, the Dynes parameter can be related to Γ , according to $\Gamma = \sqrt{\gamma_{\text{Dynes}}^2 / (\gamma_{\text{Dynes}}^2 + 1)}$. We see

in particular that the two parameters coincide $\gamma_{\text{Dynes}} = \Gamma$ whenever $\Gamma, \gamma_{\text{Dynes}} \ll 1$. This shows that fluctuations of a high-temperature electromagnetic environment constitute a possible microscopic source of the phenomenological Dynes parameter.

B. Weak and Strong Coupling

As we have seen above, the strength of the coupling between the NIS junction and the environment is determined by the function $J(t)$. Let us assume that this function is small, in a sense to be detailed below. Expanding the exponential function $\exp[J(t)]$ up to the first order in $J(t)$, Eq. (3) becomes

$$P(E) \simeq \frac{1}{2\pi\hbar} \int_{-\infty}^{+\infty} dt e^{iEt/\hbar} [1 + J(t)]. \quad (8)$$

The evaluation of the integral over time in (8) gives

$$\begin{aligned} P(E) \simeq & \delta(E) + \frac{1}{\hbar} \int_0^{+\infty} \frac{d\omega}{\omega} \frac{\Re[Z_{\text{tot}}(\omega)]}{R_K} \times \\ & \times \left\{ \left[\coth\left(\frac{1}{2}\beta_{\text{env}}\hbar\omega\right) - 1 \right] \delta\left(\frac{E}{\hbar} + \omega\right) + \right. \\ & \left. + \left[\coth\left(\frac{1}{2}\beta_{\text{env}}\hbar\omega\right) + 1 \right] \delta\left(\frac{E}{\hbar} - \omega\right) - \right. \\ & \left. - 2\hbar \coth\left(\frac{1}{2}\beta_{\text{env}}\hbar\omega\right) \delta(E) \right\}. \quad (9) \end{aligned}$$

We see that the function $P(E)$ has an elastic contribution and an inelastic one involving the exchange of at most one photon between the junction and the environment. In fact the first and the fourth terms represent the elastic tunneling involving zero and one virtual photon, respectively. The second and third terms are related to the process of absorption and emission of one real photon, respectively. We define this one-photon regime as weak coupling. On the other hand, the coupling becomes strong whenever the single-photon exchange between the junction and the environment is no longer the dominant effect. In this case, the higher-order terms cannot be neglected in the series expansion of $\exp[J(t)]$, indicating that multi-photon processes have to be taken into account.

We proceed by determining the time interval where the expansion (8) holds. Given the fact that $J(t=0) = 0$, we expect this to be the short time interval¹⁸. We set $Z(\omega) = R$ for simplicity and introduce the dimensionless time $\tau = t/R_K C$ as well as the ratio $\rho = R/R_K$. The quantity $\exp\{\Re[J(\tau, \rho)]\}$ decays monotonically with

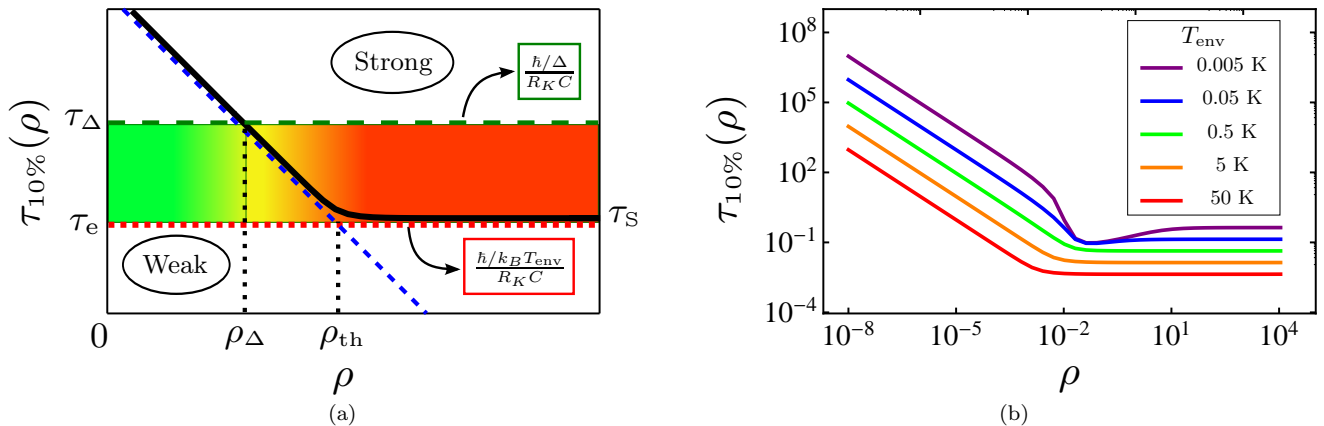


FIG. 2: Plot of the separatrix $\tau_{10\%}(\rho)$ as a function of the dimensionless resistance $\rho = R/R_K$, defined as the solution of the equation $\exp\{\Re[J(\tau_{10\%}, \rho)]\} = 0.9$ with C fixed. Both plots are in double logarithmic scale. (a) For a fixed value of T_{env} , $\tau_{10\%}(\rho)$ separates the weak and strong coupling regions (black thick line). The colored strip indicates the time interval bound by $\tau_\Delta = \hbar/\Delta R_K C$ (dark green dashed line) and $\tau_e = \hbar/k_B T_{\text{env}} R_K C$ (red dashed line). The intersection between τ_Δ and the separatrix $\tau_{10\%}(\rho)$ defines the resistance ρ_Δ . The asymptotic expression for $\tau_{10\%}(\rho)$ valid for $\rho \rightarrow 0$ and proportional to $1/\rho$ is also shown (blue dashed line). Its intersection with the line corresponding to $\tau_S \sim \sqrt{\hbar/k_B T_{\text{env}} R_K C}$ defines the threshold resistance ρ_{th} . On the logarithmic scale used here, τ_S almost coincides with τ_e . (b) As the temperature of the environment, T_{env} , is decreased, the curve $\tau_{10\%}(\rho)$ moves up, thereby increasing the weak coupling region.

increasing time τ , starting from unity at $\tau = 0$. The rate at which it decays depends on ρ : the larger ρ , the faster it decays, in agreement with Ref. 18. We determine the relevant short time interval by determining the characteristic time $\tau_{10\%}$, at which the quantity $\exp\{\Re[J(\tau, \rho)]\}$ dropped by 10%. Figure 2(a) shows $\tau_{10\%}$ as a function of the parameter ρ , keeping T_{env} and C fixed. The line $\tau_{10\%}(\rho)$ separates the weak coupling regime found at short times from the strong coupling regimes reached for longer times. As expected¹⁸, with increasing ρ , the separatrix $\tau_{10\%}(\rho)$ decreases as $1/\rho$, and then saturates at a value $\tau_S \sim \sqrt{\hbar/k_B T_{\text{env}} R_K C}$ for $\rho > \rho_{\text{th}} \sim \tau_S$. As shown in Fig. 2(b), the curve $\tau_{10\%}(\rho)$ shifts up when decreasing the temperature of the environment, T_{env} , thereby increasing the time interval where the expansion (8) holds.

We now return to the inelastic tunneling of single electrons through the NIS junction. Under subgap conditions $k_B T_{\text{jun}}, eV \ll \Delta$, the energy E relevant for the photon-assisted tunneling processes is in the interval $\Delta \lesssim E \lesssim k_B T_{\text{env}}$. The upper bound corresponds to the largest energy the junction can absorb from the environment. In time domain, we thus have to consider the interval $\tau_e < \tau < \tau_\Delta$ where $\tau_\Delta = \hbar/\Delta R_K C$ and $\tau_e = \hbar/k_B T_{\text{env}} R_K C$. This interval is represented by the colored strip in Fig. 2(a). Note that on the logarithmic scale used here, the lower bound τ_e almost coincides with the value τ_S at which the separatrix saturates for large values of ρ . The intersection between τ_Δ and the 10% curve $\tau_{10\%}(\rho)$ defines the characteristic resistance ρ_Δ separating the weak and strong coupling regimes. When $\rho < \rho_\Delta$, coupling is weak and only single-photon absorption processes occur (green area); if $\rho \sim \rho_\Delta$ both single- and multi-photon processes occur during single-electron tunneling (yellow-orange area); as soon as $\rho \gg \rho_\Delta$, multi-

photon processes become dominant (red area). In particular, the two limiting cases $\rho \ll \rho_\Delta, \rho_{\text{th}}$ and $\rho \gg \rho_\Delta, \rho_{\text{th}}$ are equivalent to the conditions $R/R_K \ll \Delta/k_B T_{\text{env}}$ and $R/R_K \gg \Delta/k_B T_{\text{env}}$ respectively.

C. Subgap Leakage Current: Weak Coupling

We start by dealing with the weak coupling case. Since we are interested in the subgap region of the I - V characteristic, $k_B T_{\text{jun}}, eV \ll \Delta$, the behavior of the function $P(E)$ at energies $E > -\Delta$ is irrelevant. Therefore we can ignore the elastic contributions in Eq. (9). Evaluating the integral over frequencies in Eq. (9), the relevant contribution to the function $P(E)$ for energies $E \neq 0$ reads

$$P(E) \simeq 2 \frac{\Re[Z_{\text{tot}}(E/\hbar)]}{R_K} \left(\frac{1+n(E)}{E} \right). \quad (10)$$

Here $n(E) = [e^{\beta_{\text{env}} E} - 1]^{-1}$ is the Bose-Einstein distribution of the photons of the environment.

The probability density (10) can be used to get a limiting expression for Γ ,

$$\Gamma = 4 \int_{\Delta}^{+\infty} dE N_S(E) \frac{\Re[Z_{\text{tot}}(E/\hbar)]}{R_K} \frac{n(E)}{E}. \quad (11)$$

Let us apply this result to the example of a purely resistive external environment. This model has been used before to study devices based on tunnel junctions in connection with experiments^{16,19,20}. Replacing the external impedance $Z(\omega)$ of the circuit of Fig. 1(a) by a pure re-

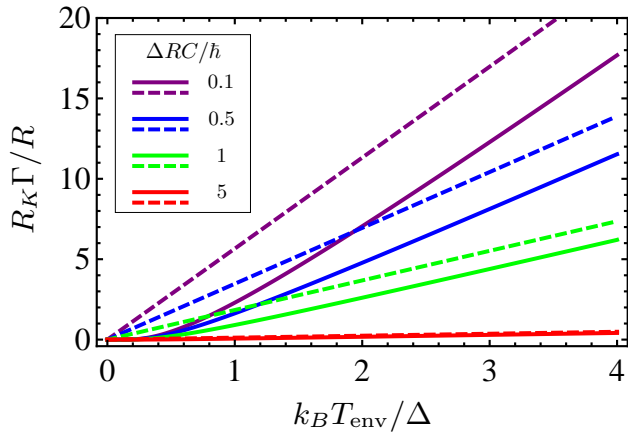


FIG. 3: Plot of the rescaled parameter $R_K \Gamma / R$ as a function of $k_B T_{\text{env}} / \Delta$ for different values of the ratio $\Delta RC / \hbar$. Solid lines are obtained by a numerical integration of Eq. (11) using Eq. (12). Dashed lines refer to the asymptotic Γ given by Eq. (13).

sistance R , the real part of the total impedance is

$$\Re[Z_{\text{tot}}(\omega)] = \frac{R}{1 + (\omega RC)^2}. \quad (12)$$

Numerical integration of Eq. (11) using Eq. (12) is straightforward. Results for $R_K \Gamma / R$ as a function of $k_B T_{\text{env}} / \Delta$ are shown in Fig. 3 for various values of the parameter $\Delta RC / \hbar$. We see that Γ increases monotonically with temperature. Also shown is the asymptotic linear temperature dependence of Γ reached for temperatures $k_B T_{\text{env}} \gg \Delta$,

$$\Gamma \simeq 2\pi \frac{R}{R_K} \frac{k_B T_{\text{env}}}{\Delta} \left[1 - \frac{\Delta RC / \hbar}{\sqrt{1 + (\Delta RC / \hbar)^2}} \right]. \quad (13)$$

As the parameter $\Delta RC / \hbar$ is increased, the slope characterizing the limiting dependence decreases: photon-assisted inelastic tunneling is effectively reduced by increasing the junction capacitance. Note that in the limit $\Delta RC / \hbar \ll 1$ the result (13) tends to $\Gamma = 2\pi(R/R_K)(k_B T_{\text{env}}/\Delta)$, obtained in Ref. 16.

D. Subgap Leakage Current: Strong Coupling

We do not aim to present a general analysis in the strong coupling limit. In the particular case where $\Re[Z_{\text{tot}}(\omega)]$ is strongly peaked around $\omega = 0$, the probability density $P(E)$ can be calculated explicitly¹⁸ and results for the parameter Γ obtained. Let us illustrate this by considering a purely resistive environment. When the resistance is big, $R \gg R_K \Delta / k_B T_{\text{env}}$ (see Sec.IIB), the impedance (12) becomes

$$\Re[Z_{\text{tot}}(\omega)] \simeq \left(\frac{\pi}{C} \right) \delta(\omega). \quad (14)$$

As a result, the function $P(E)$ is given by

$$P(E) \simeq \frac{1}{\sqrt{4\pi k_B T_{\text{env}} E_C}} \exp \left[-\frac{(E - E_C)^2}{4k_B T_{\text{env}} E_C} \right]. \quad (15)$$

Here we defined the charging energy $E_C = e^2/2C$. Inserting the function (15) in equation (7), we find

$$\Gamma = \frac{1}{\sqrt{\pi E_C k_B T_{\text{env}}}} \int_{\Delta}^{+\infty} dE N_S(E) \times \exp \left[-\frac{(E + E_C)^2}{4E_C k_B T_{\text{env}}} \right]. \quad (16)$$

Note that this result depends on R implicitly only, through the requirement $R \gg R_K \Delta / k_B T_{\text{env}}$. Direct numerical integration of (16) yields Γ as a function of $k_B T_{\text{env}} / \Delta$ and E_C / Δ , as shown in Figs. 4(a) and 4(b). Some remarks are in order at this point. First of all, for $E_C \ll \Delta$, the integral in Eq. (16) can be evaluated approximately, $\Gamma \simeq e^{-\Delta^2/k_B T_{\text{env}} E_C}$. As in the weak coupling regime, large values of the capacitance lead to a reduction of the parameter Γ . Upon increasing the ratio E_C / Δ , Γ will first increase, then it decreases again when $E_C / \Delta > 1$, which is a manifestation of the Coulomb blockade. As a function of temperature, Γ increases monotonically, similarly to the weak coupling limit. However, rather than reaching an asymptotic linear dependence, Γ saturates at $\Gamma = 1$ for temperatures $k_B T_{\text{env}} E_C \gg \Delta^2$: the noise is so strong that features of the order of the gap Δ are washed out.

III. NIS JUNCTION COUPLED TO A HIGH-TEMPERATURE ENVIRONMENT BY MEANS OF A TRANSMISSION LINE

In the previous section we have studied the subgap leakage current in a NIS junction which is directly coupled to the external environment $Z(\omega)$. We have seen that a reduction of the subgap leakage current is possible when the capacitance of the junction, C , is increased and/or the resistance of the environment, R , is decreased. Unfortunately, in real experiments R , and in particular C , cannot be chosen arbitrarily and one needs other means to achieve the accuracy requirements for the aforementioned NIS junction's applications. We therefore consider the circuit of Fig. 1(b) where the junction is indirectly coupled to the external environment via a cold, lossy transmission line acting as a filter.

A. Voltage Fluctuations in the Presence of a Transmission Line

In order to find the correlation function $J(t)$ in the presence of the transmission line, we solve the intermedi-

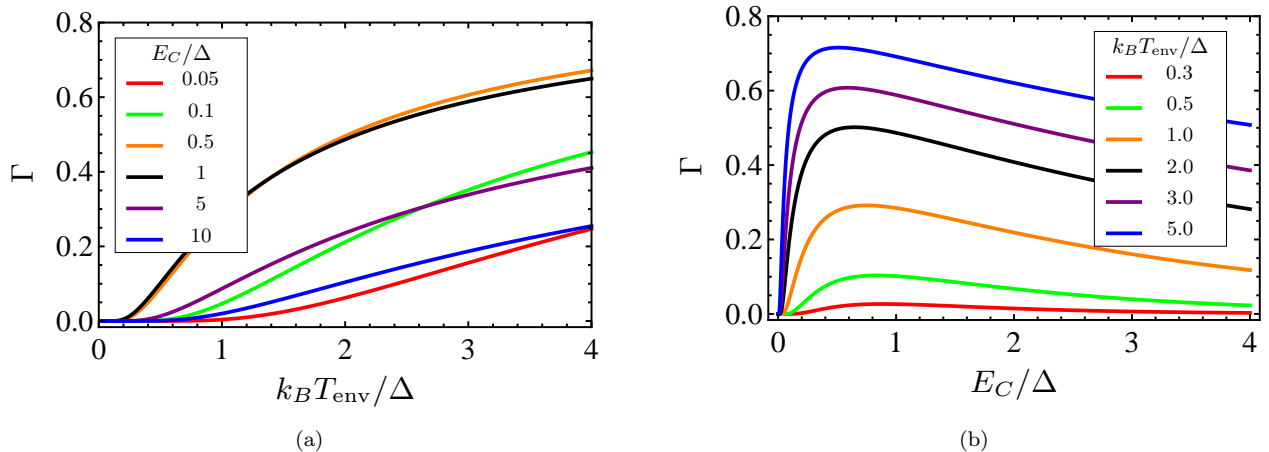


FIG. 4: (a) Plot of the parameter Γ as a function of $k_B T_{\text{env}}/\Delta$ obtained considering the numerical integration of Eq. (16). Each curve refers to a certain fixed value of the ratio E_C/Δ (see legend). (b) Numerical plot of the same quantity, Eq. (16), as a function of E_C/Δ for different values of the ratio $k_B T_{\text{env}}/\Delta$, as indicated.

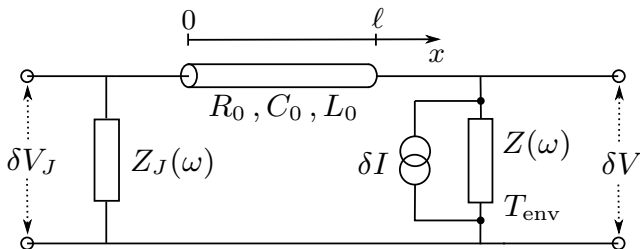


FIG. 5: Sketch of the circuit discussed in Sec. III A.

ate problem of the propagation of the noise generated by the high-temperature environment with impedance $Z(\omega)$ through the line towards the junction, as shown in Fig. 5. The line has a length ℓ and is described by the parameters R_0, C_0 and L_0 , the resistance, the capacitance and the inductance per unit length respectively. We ignore the thermal noise produced by the impedance $Z_J(\omega)$ and by the line, assuming both components at zero temperature. The high-temperature element produces current noise δI which in turn induces voltage noise δV .

To understand how the potential drop δV_J across $Z_J(\omega)$ is connected to $\delta V = Z(\omega)\delta I$, we start considering the potential $V(x)$ and the current $I(x)$ at a given point x along the transmission line. They satisfy the two partial differential equations,

$$\begin{aligned} \frac{\partial V(x)}{\partial x} &= -I(x) [R_0 - i\omega L_0], \\ \frac{\partial I(x)}{\partial x} &= i\omega C_0 V(x). \end{aligned}$$

Combining them one obtains the wave equation

$$\frac{\partial^2 V(x)}{\partial x^2} = -K^2(\omega) V(x), \quad (17)$$

where $K^2(\omega) = \omega^2 L_0 C_0 + i\omega R_0 C_0$ is the wave vector squared of the signal which propagates along the line. A

general solution of Eq. (17) is given by

$$V(x) = A e^{iK(\omega)x} + B e^{-iK(\omega)x}. \quad (18)$$

Consequently the current along the line is

$$I(x) = \frac{1}{Z_\infty(\omega)} [A e^{iK(\omega)x} - B e^{-iK(\omega)x}], \quad (19)$$

with $Z_\infty(\omega) = i(R_0 - i\omega L_0)/K(\omega)$. The parameters A and B can be determined by means of the boundary conditions

$$\begin{aligned} V(\ell) &= Z(\omega) [I(\ell) + \delta I] = Z(\omega) I(\ell) + \delta V \\ V(0) &= -Z_J(\omega) I(0). \end{aligned}$$

As a result, the potential drop $\delta V_J = V(0) = A + B$ across the impedance $Z_J(\omega)$ depends on the noise δV according to the relation

$$\delta V_J = T(\omega) \delta V. \quad (20)$$

In this last equation we introduced $T(\omega)$, the transmission function

$$\begin{aligned} T(\omega) &= \frac{2 Z_\infty(\omega) Z_J(\omega)}{[Z_\infty(\omega) + Z(\omega)] [Z_\infty(\omega) + Z_J(\omega)]} \times \\ &\times \frac{1}{e^{-iK(\omega)\ell} - \lambda_1(\omega) \lambda_2(\omega) e^{iK(\omega)\ell}}, \end{aligned} \quad (21)$$

where

$$\lambda_1(\omega) = \frac{Z_\infty(\omega) - Z(\omega)}{Z_\infty(\omega) + Z(\omega)} \quad \lambda_2(\omega) = \frac{Z_\infty(\omega) - Z_J(\omega)}{Z_\infty(\omega) + Z_J(\omega)}$$

are the reflection coefficients. Assuming that the potential δV satisfies the quantum fluctuation-dissipation theorem,

$$\langle \delta V(t) \delta V(0) \rangle_\omega = 2\hbar\omega \frac{\Re[Z(\omega)]}{1 - e^{-\beta_{\text{env}}\hbar\omega}},$$

the spectral density function of the potential (20) is

$$\left\langle \delta V_J(t) \delta V_J(0) \right\rangle_\omega = \left| T(\omega) \right|^2 2\hbar\omega \frac{\Re[Z(\omega)]}{1 - e^{-\beta_{\text{env}}\hbar\omega}}. \quad (22)$$

This expression describes the propagation of the noise from $Z(\omega)$ to the noiseless impedance $Z_J(\omega)$ through the noiseless transmission line.

B. Correlation Function for the Transmission Line Circuit

We use Eq. (22) to calculate the modified correlation function $J_T(t)$ which appears in Eq. (3). According to Ref. 18, $J(t)$ is defined as the correlation function

$$J(t) \equiv \left\langle \varphi_J(t)\varphi_J(0) - \varphi_J(0)\varphi_J(t) \right\rangle, \quad (23)$$

where the phase $\varphi_J(t)$ is the time integral of the potential $\delta V_J(t)$ across the NIS junction,

$$\varphi_J(t) \equiv \frac{e}{\hbar} \int_{-\infty}^t \delta V_J(\tau) d\tau.$$

In other words

$$\left\langle \varphi_J(t) \varphi_J(0) \right\rangle_\omega = \left(\frac{e}{\hbar} \right)^2 \frac{1}{\omega^2} \left\langle \delta V_J(t) \delta V_J(0) \right\rangle_\omega. \quad (24)$$

Using the fluctuation-dissipation relation (22) in (24), we rewrite Eq. (23) as a function of $T(\omega)$, $Z(\omega)$ and T_{env} . Taking the impedance $Z_J(\omega)$ to be the one of a capacitance C , the modified function $J_T(t)$ reads

$$J_T(t) = 2 \int_0^{+\infty} \frac{d\omega}{\omega} \left| T_C(\omega) \right|^2 \frac{\Re[Z(\omega)]}{R_K} \times \left\{ \coth \left(\frac{1}{2} \beta_{\text{env}} \hbar \omega \right) \left[\cos(\omega t) - 1 \right] - i \sin(\omega t) \right\}. \quad (25)$$

Here $T_C(\omega)$ is the function $T(\omega)$, Eq. (21), with $Z_J(\omega) = Z_C(\omega) = -1/i\omega C$. Since the transmission line is considered noiseless, its temperature T_{line} should be low, $T_{\text{line}} \ll \Delta/k_B$. In what follows we set $T_{\text{line}} = T_{\text{junc}} = 0$.

C. The Transmission Function

In order to understand the effect of the insertion of the transmission line in the circuit of Fig. 1(a), a discussion about the general behavior of $T_C(\omega)$ is necessary. In general, the modulus squared of the transmission function (21) is characterized by a series of resonance peaks, whose properties depend on ℓ , R_0 , C_0 , and L_0 as well as on the external impedance $Z(\omega)$. To have an idea of the behavior of $|T_C(\omega)|^2$, let us consider the case of a purely resistive environment, $Z(\omega) = R$.

Figure 6 illustrates the behavior of $|T_C(\omega)|^2$ as a function of ωRC for different values of the dimensionless parameters $z_0 = \sqrt{L_0/C_0}/R$, $c_0 = \ell C_0/C$ and $r_0 = \ell R_0/R$. Also shown is the Lorentzian result

$$\left| T_C(\omega) \right|^2 = 1/[1 + (\omega RC)^2] \quad (26)$$

found for $\ell = 0$, *i.e.*, in the absence of the transmission line. In order for the line to be an efficient filter, we require $|T_C(\omega)|^2$ to be below this Lorentzian curve in the relevant frequency ranges. We see that both the position and the width of the resonance peaks are proportional to $\pi/2c_0z_0$: the longer is the transmission line, the denser around zero and the sharper are the peaks. Their height decreases rapidly as the dimensionless frequency ωRC is increased. This can be seen in particular when the line has no losses, $r_0 = 0$, see Figs. 6(a) – 6(d). Although the Lorentzian curve is approached for lossless lines when c_0 or z_0 is reduced, we observe no real reduction below it.

A significant reduction of the height of the peaks is possible if the line which connects the NIS junction and the environment is lossy, $r_0 > 0$. Indeed, we see from Figs. 6(e) and 6(f) that the bigger is r_0 the smaller are the local maxima of $|T_C(\omega)|^2$. Moreover, the transmission function is even much smaller than $1/[1 + (\omega RC)^2]$ when the condition $r_0 \gg z_0$ is satisfied, as is seen in Figs. 6(f) and 7. Therefore, within this particular limit, the insertion of a resistive transmission line may be convenient.

D. Subgap Leakage Current: Weak Coupling

We expect that the single- and multi-photon regimes, weak and strong coupling respectively, are strongly related to the resistance per unit length, R_0 . Let us analyze the situation proceeding as in Sec.II B. We consider the function $\tau_{10\%}(\rho)$ for a purely resistive environment. In Fig. 8 we plot $\tau_{10\%}(\rho)$ as a function of the dimensionless resistance ρ for different values of R_0 . We see that the lossier the transmission line is, the more the weak coupling region spreads out. The resistance ρ_Δ , given by the intersection between $\tau_{10\%}(\rho)$ and the line corresponding to the dimensionless time $\tau_\Delta = \hbar/\Delta R_K C$, significantly shifts towards higher values of ρ as R_0 is increased; the lossy line indeed protects the junction from the high-temperature external environment. Hereafter, we will therefore focus on a highly resistive transmission line and only the weak coupling regime will be treated.

With the help of Eq. (25), the function $P(E)$ for the circuit of Fig. 1(b) can be obtained in the weak coupling regime. Proceeding as in Sec. II C, we find

$$P(E) \simeq 2 \left| T_C(E/\hbar) \right|^2 \frac{\Re[Z(E/\hbar)]}{R_K} \left(\frac{1 + n(E)}{E} \right). \quad (27)$$

Evaluating the relation (27) for negative energies and inserting the result into Eq. (7), the parameter Γ can be

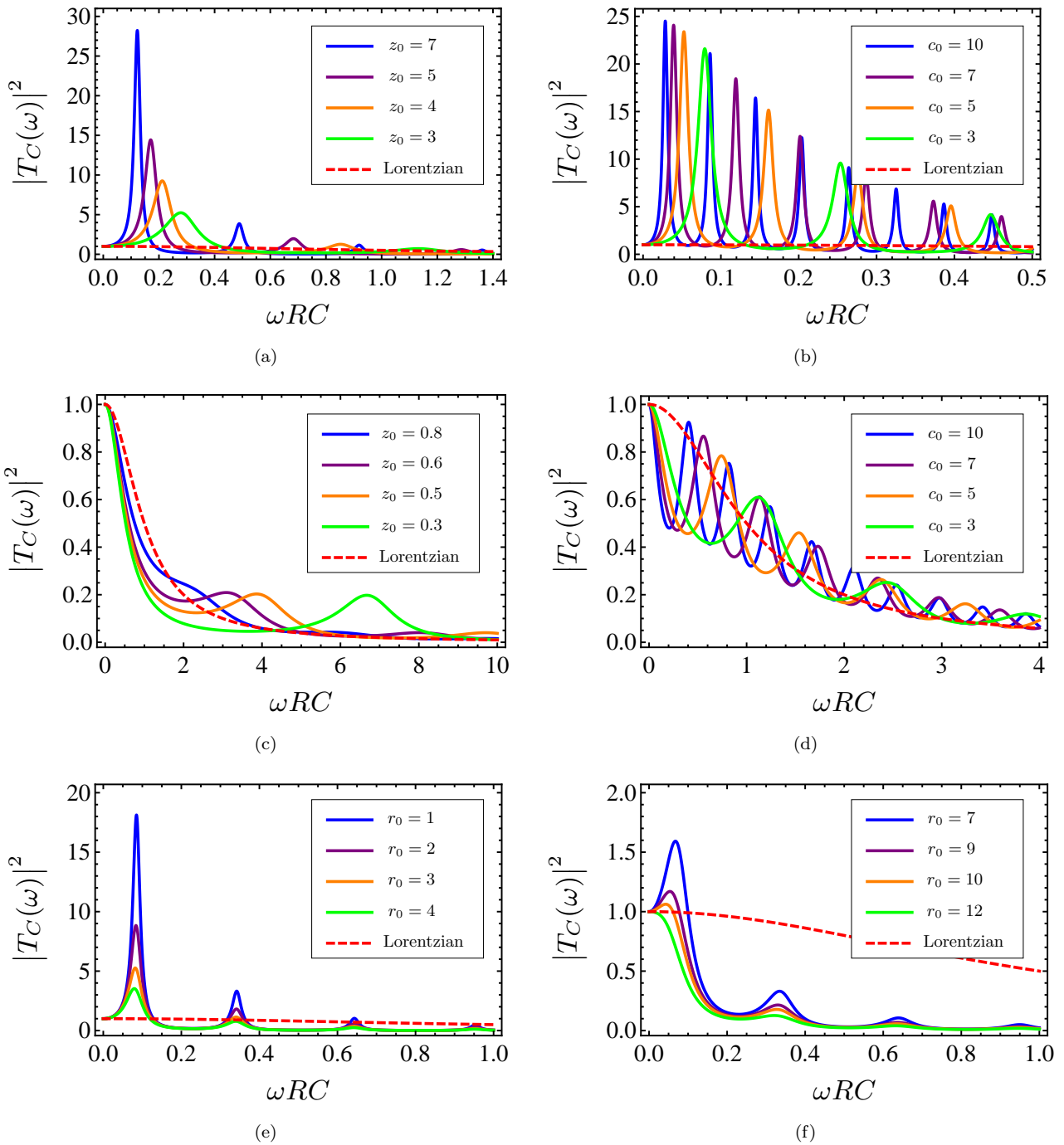


FIG. 6: Plots of the transmission function $|T_C(\omega)|^2$ as a function of the dimensionless variable ωRC . Each panel corresponds to a different set of the parameters z_0 , c_0 and r_0 : (a) $r_0 = 0$, $c_0 = 1$, $z_0 = (7, 5, 4, 3)$; (b) $r_0 = 0$, $z_0 = 5$, $c_0 = (10, 7, 5, 3)$; (c) $r_0 = 0$, $c_0 = 1$, $z_0 = (0.8, 0.6, 0.5, 0.3)$; (d) $r_0 = 0$, $z_0 = 0.7$, $c_0 = (10, 7, 5, 3)$; (e) $z_0 = 10$, $c_0 = 1$, $r_0 = (1, 2, 3, 4)$; (f) $z_0 = 10$, $c_0 = 1$, $r_0 = (7, 9, 10, 12)$.

written as

$$\Gamma = 4 \int_{\Delta}^{+\infty} dE N_S(E) |T_C(E/\hbar)|^2 \frac{\Re[Z(E/\hbar)]}{R_K} \frac{n(E)}{E}. \quad (28)$$

We next specialize to the case of large resistance per

unit length, R_0 . In order to obtain a limiting expression for $|T_C(\omega)|^2$ for $R_0 \rightarrow \infty$, let us assume that the inductive properties of the line are negligible compared to R_0 . Since the relevant frequency scale is given by Δ/\hbar , this means that the condition $R_0 \gg L_0 \Delta/\hbar$ should

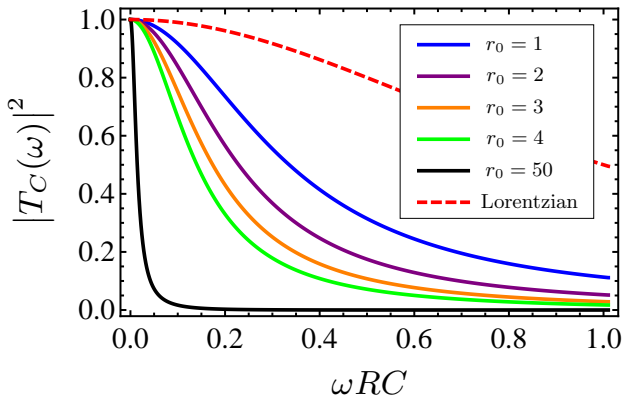


FIG. 7: Plot of the transmission function $|T_C(\omega)|^2$ as a function of the dimensionless variable ωRC for different values of the parameter r_0 . The other parameters are: $c_0 = 1$, $z_0 = 0.7$. Also shown is the Lorentzian corresponding to the function $|T_C(\omega)|^2$ in the limit $\ell \rightarrow 0$, given by Eq. (26).

hold. Within this RC limit, we find that the wave vector $K(\omega)$ of the signal propagating through the transmission line has an imaginary part equal to $\sqrt{\omega R_0 C_0}/2$. As a result, the amplitude of the noise is exponentially attenuated along the line (see Eqs. (18) and (19)) being proportional to $\exp[-\ell\sqrt{2\omega R_0 C_0}]$. We see that the bigger ℓ and R_0 are, the smaller is the voltage noise which reaches the junction. In particular, an exponential suppression of the propagating signal is achieved when the inequality $\ell\sqrt{2\Delta R_0 C_0}/\hbar \gg 1$ is valid as well. This additional condition allows us to write the equation

$$\left| e^{-iK(\omega)\ell} - \lambda_1(\omega) \lambda_2(\omega) e^{iK(\omega)\ell} \right|^2 \simeq 4 e^{\ell\sqrt{2\omega R_0 C_0}}.$$

Then the modulus squared of the transmission function $T_C(\omega)$ becomes

$$\left| T_C(\omega) \right|^2 \simeq \left| \frac{Z_\infty(\omega) Z_C(\omega) e^{-\ell\sqrt{2\omega R_0 C_0}/2}}{[Z_\infty(\omega) + Z(\omega)][Z_\infty(\omega) + Z_C(\omega)]} \right|^2 \quad (29)$$

where $Z_\infty(\omega) \simeq (1+i)\sqrt{R_0/2\omega C_0}$ for a line in the RC limit. Combining the two conditions used so far, we find that the approximated function (29) holds when the resistance of the transmission line, ℓR_0 , is much bigger than its characteristic impedance $Z_\infty = \sqrt{L_0/C_0}$.

Increasing the resistance per unit length, R_0 , one also expects that interference effects become negligible. Indeed, when R_0 is very big, the amplitude of the signal across the junction is much smaller than its starting value and its reflected counterpart vanishes rapidly before reaching the noise source again. In terms of our description of the transmission line given in Sec. III A, this happens when the reflection coefficients $\lambda_1(\omega)$ and $\lambda_2(\omega)$ tend to 1. In fact, in this limit, the potential drop (18) tends to 0 across the junction and to δV across the impedance $Z(\omega)$. For a purely resistive environment, this

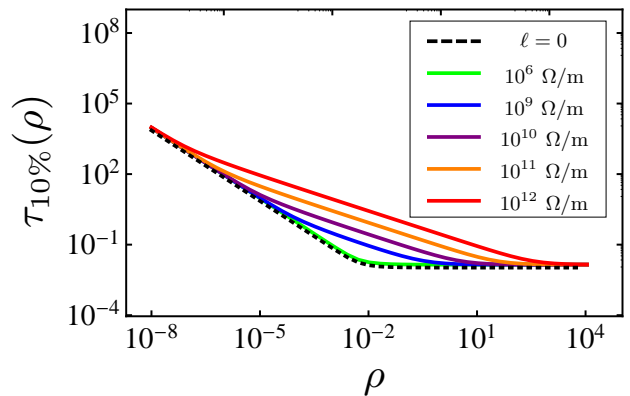


FIG. 8: Plot of the dimensionless time $\tau_{10\%}(\rho)$ as a function of the dimensionless resistance $\rho = R/R_K$ for different values of the resistance per unit length, R_0 , of the transmission line (see legend). Also shown is the curve $\tau_{10\%}(\rho)$, valid for the circuit of Fig. 1(a) (black dashed line). The value of the other parameters are: $\Delta \simeq 200 \mu\text{eV}$ (energy gap of Aluminum), $T_{\text{env}} = 5 \text{ K}$, $C = 10 \text{ fF}$, $C_0 = 6 \epsilon_0$, $L_0 = \mu_0$, $\ell = 10 \mu\text{m}$.

regime is reached when R_0 is such that the two inequalities $R^2 \ll \hbar R_0/2C_0\Delta$ and $\Delta R_0 C^2/\hbar C_0 \gg 2$ hold, in other words, when the resistance of the environment, R , is much smaller than $R_0 C/2C_0$. Equation (29) reduces to the asymptotic expression

$$\left| T_C(\omega) \right|^2 \simeq \frac{e^{-\ell\sqrt{2\omega R_0 C_0}}}{1 + \omega R_0 C^2/C_0}.$$

By means of this last relation, the integral in Eq. (28) can be evaluated approximately with the result

$$\Gamma \simeq 4 \frac{R}{R_K} \frac{1}{e^{\Delta/k_B T_{\text{env}}} - 1} \times \sqrt{\frac{\pi}{\ell\sqrt{2\Delta R_0 C_0}/\hbar}} \frac{e^{-\ell\sqrt{2\Delta R_0 C_0}/\hbar}}{1 + \Delta R_0 C^2/\hbar C_0}. \quad (30)$$

We see that this asymptotic parameter Γ decreases exponentially in terms of ℓ and R_0 ; the dependence on the junction capacitance C is rather weak. The insertion of a highly resistive and noiseless transmission line between the NIS junction and the high-temperature environment indeed helps to suppress the subgap leakage current. The plot of Fig. 9 shows the exponential decay for a set of values of R_0 and ℓ that can be used in real experiments. Particularly interesting is the region where $10^8 \Omega/\text{m} \lesssim R_0 \lesssim 10^{10} \Omega/\text{m}$ and $10 \mu\text{m} \lesssim \ell \lesssim 10^2 \mu\text{m}$. A transmission line with these values of R_0 and ℓ allows one to go far below $\Gamma \simeq \gamma_{\text{dynes}} \sim 10^{-7}$, *i.e.*, a value of Γ which guarantees the achievement of the accuracy requirements for the superconducting gap-based technological applications of the NIS junction⁹.

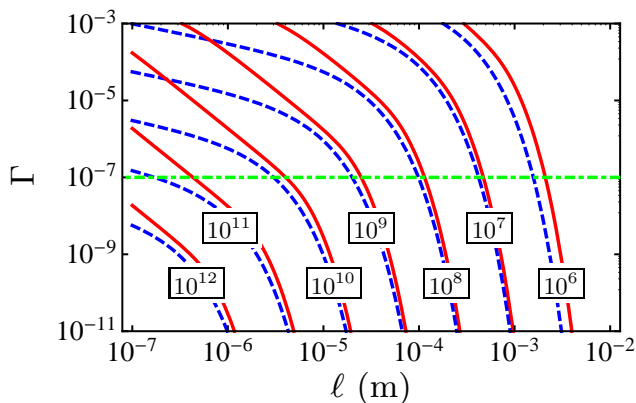


FIG. 9: Plot of the parameter Γ , Eq. (28), as a function of the length of the transmission line ℓ . The red solid line is obtained by means of the numerical integration of Eq. (28) for a purely resistive environment. The blue dashed line is the plot of the asymptotic parameter given by the Eq. (30). These two curves are plotted for different values of the resistance per unit length R_0 (Ω/m) (as indicated in the graph). All the plots are obtained considering the gap parameter of the aluminum, $\Delta \simeq 200 \mu\text{eV}$. The other parameters are: $T_{\text{env}} = 5 \text{ K}$, $C = 10 \text{ fF}$, $R = 10 \Omega$, $C_0 = 6 \varepsilon_0$, $L_0 = \mu_0$.

IV. MULTI-PARTICLE TUNNELING

Our analysis focuses on the single-particle subgap current through the NIS junction. We ignore the contribution due to higher order processes in tunneling, such as Andreev reflection^{12–14}. Hence, in order to establish the validity of our single-particle tunneling assumption, one has to compare the parameter Γ characterizing the leakage current with the dimensionless Andreev subgap conductance $g_A = G_A R_T$. In ballistic junctions, second-order perturbation theory yields the standard two-particle subgap conductance

$$G_A \simeq R_K / [R_T^2 (k_F^2 S)], \quad (31)$$

where $k_F^2 S$ is the number of conduction channels in the tunnel barrier. Two-electron tunneling can be ignored as long as $\Gamma > R_K / R_T k_F^2 S$. Typical estimates¹⁴ yield $R_K / R_T k_F^2 S \sim 10^{-7}$.

On the other hand, in the diffusive case the electrons reflected by the barrier are backscattered by the impurities randomly situated close to the barrier in the normal metal. Interference between the electrons in a region characterized by the coherence length $\xi_N =$

$\sqrt{\hbar D / \max\{eV, k_B T_{\text{jun}}\}}$, where D is the diffusion coefficient, affects the two-particle tunneling probability²¹. As a result, G_A is given by

$$G_A \simeq R_N / R_T^2 \quad (32)$$

where R_N is the resistance of the diffusive normal metal over a length ξ_N . General estimates are hard to give in this situation, since the result is strongly geometry-dependent; the condition $\Gamma > R_N / R_T$ will be more stringent than the one for the ballistic case, especially under subgap conditions where ξ_N and hence R_N can be large.

Should Andreev reflection become dominant, one can always suppress it efficiently using the Coulomb blockade feature¹⁴ that suppresses two-particle tunneling more strongly than single-particle tunneling.

V. CONCLUSIONS

In conclusion, we studied the single-particle tunneling current through a voltage-biased NIS junction. Due to the presence of the superconducting energy gap Δ in the BCS density of states, when the junction is kept at the temperature $T_{\text{jun}} \ll \Delta / k_B$ no current is expected to flow within the subgap region $-\Delta < eV < \Delta$. Actually, even if the higher order tunneling processes are suppressed, a small subgap current is still measured experimentally. This leakage current limits the accuracy in applications involving NIS junctions. The origin of the leakage current is the exchange of energy exceeding the gap Δ between the junction and the external high-temperature environment in which it is embedded. We studied this mechanism analytically and numerically. In particular, we found that a cold and lossy transmission line inserted between the junction and the environment reduces exponentially the subgap leakage current acting as a filter. This indirect configuration helps to achieve the required suppression of noise.

Acknowledgments. The authors thank W. Belzig and G. Rastelli for useful discussions. Financial support from the Marie Curie Initial Training Network (ITN) Q-NET (project no. 264034), from Institut Universitaire de France and from Aalto University's ASCI visiting professor programme is gratefully acknowledged. The work was partially supported by the Academy of Finland through its LTQ (project no. 250280) COE grant (VFM and JPP), and the National Doctoral Programme in Nanoscience, NGS-NANO (VFM).

¹ H. Pothier, S. Guéron, Norman O. Birge, D. Esteve, and M. H. Devoret, Phys. Rev. Lett. **79**, 3490 (1997).

² H. Courtois, M. Meschke, J. T. Peltonen, and J. P. Pekola, Phys. Rev. Lett. **101**, 067002 (2008).

³ F. Giazotto, T. T. Heikkilä, A. Luukanen, A. M. Savin, and J. P. Pekola, Rev. Mod. Phys. **78**, 217 (2006).

⁴ J. M. Rowell and D. C. Tsui, Phys. Rev. B **14**, 2456 (1976).

⁵ D. R. Schmidt, C. S. Yung, and A. N. Cleland, Appl. Phys. Lett. **83**, 1002 (2003).

⁶ N. Nahum, T. M. Eiles, and John M. Martinis, Appl. Phys. Lett. **65**, 3123 (1994).

⁷ M. M. Leivo, J. P. Pekola, and D. V. Averin, Appl. Phys.

- Lett. **68**, 1996 (1996).
- ⁸ A. Kemppinen, M. Meschke, M. Möttönen, D. V. Averin, and J. P. Pekola, Eur. Phys. J. Special Topics **172**, 311 (2009).
- ⁹ J. P. Pekola, O.-P. Saira, V. F. Maisi, A. Kemppinen, M. Möttönen, Yu. A. Pashkin, D. V. Averin, Rev. Mod. Phys. (to be published), arXiv:1208.4030 (2012).
- ¹⁰ J. Bardeen, L. N. Cooper, and J. R. Schrieffer, Phys. Rev. **108**, 1175 (1957).
- ¹¹ I. Giaever, H. R. Hart, Jr., and K. Megerle, Phys. Rev. **126**, 941 (1962).
- ¹² A. F. Andreev, Zh. Eksp. Teor. Fiz. **46**, 1823 (1964) [Sov. Phys. JETP **19**, 1228 (1964)].
- ¹³ G. E. Blonder, M. Tinkham, and T. M. Klapwijk, Phys. Rev. B **25**, 4515 (1982).
- ¹⁴ V. F. Maisi, O.-P. Saira, Yu. A. Pashkin, J. S. Tsai, D. V. Averin, and J. P. Pekola, Phys. Rev. Lett. **106**, 217003 (2011).
- ¹⁵ R. C. Dynes, V. Narayanamurti, and J. P. Garno, Phys. Rev. Lett. **41**, 1509 (1978).
- ¹⁶ J. P. Pekola, V. F. Maisi, S. Kafanov, N. Chekurov, A. Kemppinen, Yu. A. Pashkin, O.-P. Saira, M. Möttönen, and J. S. Tsai, Phys. Rev. Lett. **105**, 026803 (2010).
- ¹⁷ O.-P. Saira, M. Möttönen, V. F. Maisi, and J. P. Pekola, Phys. Rev. B **82**, 155443 (2010).
- ¹⁸ G. L. Ingold and Yu. V. Nazarov: *Single charge tunneling*, edited by H. Grabert and M. H. Devoret, NATO ASI Series B, **294**, 21-107 (Plenum Press, New York) (1992).
- ¹⁹ J. M. Martinis and M. Nahum, Phys. Rev. B **48**, 18316 (1993).
- ²⁰ J. M. Hergenrother, J. G. Lu, M. T. Tuominen, D. C. Ralph, and M. Tinkham, Phys. Rev. B **51**, 9407 (1995).
- ²¹ F. W. J. Hekking and Yu. V. Nazarov, Phys. Rev. Lett. **71**, 1625 (1993); Phys. Rev. B **49**, 6847 (1994).